1-1-2012

# Shock-less Hypersonic Intakes

Seyed Hossein Miri
*Ryerson University*

# SHOCK-LESS HYPERSONIC INTAKES

by

Seyed Hossein Miri, B.Eng, 1997 - Ryerson University

A Project

presented to Ryerson University

in partial fulfillment of the

requirements for the degree of

Master of Engineering

in the program of

Aerospace Engineering

Toronto, Ontario, Canada, 2012

## Author's Declaration

I hereby declare that I am the sole author of this thesis. This is a true copy of the thesis, including any required final revisions, as accepted by my examiners.

I authorize Ryerson University to lend this thesis to other institutions or individuals for the purpose of scholarly research.

I further authorize Ryerson University to reproduce this thesis by photocopying or by other means, in total or in part, at the request of other institutions or individuals for the purpose of scholarly research.

I understand that my thesis may be made electronically available to the public.

## Abstract

SHOCK-LESS HYPERSONIC INTAKES
Master of Engineering, 2012
Seyed Hossein Miri
Aerospace Engineering
Ryerson University

The accuracy of CFD for simulating hypersonic air intake flow is verified by calculating the flow inside a Busemann type intake. The CFD results are then compared against the “exact” solution for the Busemann intake as calculated from the Taylor-McColl equations for conical flow.

The method proposed by G. Emanuel (the Lens Analogy) for generating an intake shape that transforms parallel and uniform hypersonic (freestream) flow isentropically to another parallel and uniform, less hypersonic, flow has been verified by CFD (SOLVER II) simulation, based on Finite Volume Method (FVM). The shock-less (isentropic) nature of the Lens Analogy (LA) flow shapes has been explored at both on and off-design Mach numbers.

The Lens Analogy (LA) method exhibits a limit line (singularity) for low Mach number flows, where the streamlines perform an unrealistic reversal in direction. CFD calculations show no corresponding anomalies.

## Acknowledgments

Dr. Jeff Yokota provided continuing support and encouragement. His help was essential and is much appreciated.

Also essential to completion of this project has been Dr. George Emanuel from Oklahoma University. I thank Dr. Emanuel for generously sharing his knowledge and experience respecting the “Lens Analogy” concept.

I would like to extend my deepest gratitude to Professor Sannu Molder for his tireless support and technical supervision.

Table of Contents Page

List of Tables Page

List of Figures Page

List of Appendices Page

*The first hypersonic X-51 scramjet powered long-duration flights…….that tie atmospheric and space propulsion will begin as early as May 25 at Edwards Air Force Base. According to the article (17 May 2011 issue of Spaceflight Now), scramjet propulsion is the future for spaceflight as even a partially successful test would hasten progress on spacecraft that could launch horizontally. Furthermore, this is "an example of the type of revolutionary propulsion that …..will be needed for future space operations." The article noted that "there is a bright future for a range of scramjet-powered vehicles" and "scramjet development will proceed no matter what happens in the near-term shift to commercial crew and cargo launch to the International Space Station."*

A shortened version from AIAA Daily Launch, March 2011

# Introduction

A flight vehicle that is propelled by air breathing engine derives its benefit from not having to carry the oxidant necessary for burning its fuel. Instead the oxidant is supplied from the air so that any on-board oxidant mass and tankage can be replaced by useful payload. An order of magnitude advantage in operating performance is possible over that of rocket motors [1]. Air breathing engines fall into two main categories: gas turbines and ram-scramjets.

Gas turbines have been in use since the Second World War. They are directly responsible for the advance of modern air travel. Their design and engineering development is limited by turbine and combustion chamber's material properties. This has put an upper limit to the speed of gas turbine powered aircraft (Mach 3).

Ramjets have an equally long development history but their application has been hampered by their inability to provide static thrust. Once up to speed, they are more efficient than turbojet from supersonic to low hypersonic Mach numbers (2 to 5). In a ramjet fuel is mixed and burned at a subsonic Mach number.

The quest for shorter flight times in the atmosphere and velocity increases for boosting payload into the earth's orbit has promoted research and development of the scramjet engine. Its distinctive difference from the ramjet engine is that fuel in its combustor is burned at a supersonic speed (Supersonic Combustion, hence Scramjet). Scramjets operate in the hypersonic flight regime. Turbomachinery-based engines are only efficient at subsonic speeds and around M3–M4, Turbomachinery are no longer useful, and ram-style compression becomes the preferred method.

All of the above types of engines consist of an intake, a combustor and a nozzle as is seen in Figure 1.0. The purpose of an intake is to make the freestream air flow acceptable to the combustion process. This requires that the Mach number be reduced, allowing heat addition to occur with the least losses and at the same time increasing the air flow static temperature to

ensure spontaneous fuel ignition. Supersonic intakes are designed to capture and efficiently compress airflow for processing by the remaining portions of a ramjet (or scramjet) engine.

*A high performance intake is critical to obtaining even minimal scramjet engine performance. For the aerodynamicist, intake design challenges arise from shock losses, boundary layer losses and their interactions, from trade-offs between adequate compression and intake starting, from attainment of sufficient performance at off-design operation and from obtaining stable and predictable as well as tailored flows at on-and off-design conditions.* [2]

At supersonic speeds this invariably requires a converging flow passage with an increasing static pressure. Such a positive pressure gradient presents the first design challenge: How to prevent boundary layer detachment. The second challenge is: How to attain started flow in the intake. The third challenge is how to minimize shock and boundary layer losses. Many of these problems are treated in the literature on scramjets. A comprehensive review of scramjets is found in reference [3].

Flow efficiency losses in the intake are caused by presence of a boundary layer on their surfaces. These are unavoidable since surfaces are required to compress the flow. Flow losses are also caused by any shockwave that may occur in the intake flow. Prevention of shock losses requires the use of a carefully shaped intake wall surfaces. These surface shapes being dictated by flight Mach number.

It is the purpose of this report to present two intake flows: a) Busemann flow, b) Lens Analogy (LA) flow due to G. Emanuel, both of which are suitable for application in scramjet engines. These are presented for comparison and verification by CFD. First CFD will be used to calculate the flow inside a Busemann intake as predicted by Taylor-McColl equation(s). This will serve to verify the capability of the CFD (SOLVER II) code to simulate an “exact” conical flow.

The code will then be applied to the flow in the Lens Analogy (LA) surface to verify that the formulation does provide a transition from an originally uniform flow at the inlet to a final uniform flow at the exit plane and that it does so isentropically.

Future studies could include extending the study to axisymmetric intakes by utilizing the Method of Characteristic (MOC). In addition, real gas effects and boundary layer corrections could be studied in detail for wind tunnel and real scenario applications.

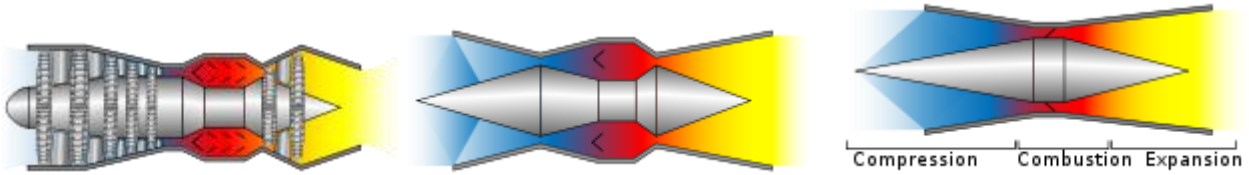


Figure 1.0 (a) turbojet (b) ramjet (c) scramjet

## 1.0 Intakes

Intakes such as Busemann flow type capture (locate) shockwaves at design locations for a specific range of operating conditions. Other intakes such as those without strong shockwave presence are suggested and the relations for their geometry are defined. A uniform hypersonic flow at a freestream inlet Mach number M1 could be transformed to a different uniform and parallel flow with an exit Mach number M2 without presence of strong shocks and losses. One such surface has been studied and formulations to generate a planar 2D surface have been outlined in reference [4].

Supersonic intakes are generally classified as: External Compression - Internal Compression - Mixed Compression - 3D Sidewall Compression - Fixed versus Variable Geometry. Both the axisymmetric Busemann intake and the planar 2-D flow outlined in LA are internal and Streamline-Traced type, where former has conical shock present by design.

## 2.0 The Busemann Intake

The Busemann flow was first described by A. Busemann [5]. It is also discussed by Courant and Friedrichs [6]. Molder and Szpiro proposed this flow for use as a scramjet intake [7]. The flow is axially and conically symmetric and hence obeys the Taylor-McColl equation for such flows. Any streamtube of the Busemann flow transforms the hypersonic freestream at its entry into a uniform and parallel stream at the exit. The isentropic compression is contained between a Mach cone on the upstream side and a shock cone on the downstream side. The conical shock then turns the flow back to uniform and parallel to the freestream into region (4). The compression and subsequent contraction of the flow from region (1) to the region (3) is accompanied by total pressure losses at the shock. The gas state in front of the conical shock is denoted by (2). The exit flow terminates with a weak conical shock hence the flow is not isentropic and some total pressure losses take place. See Figure 2.0

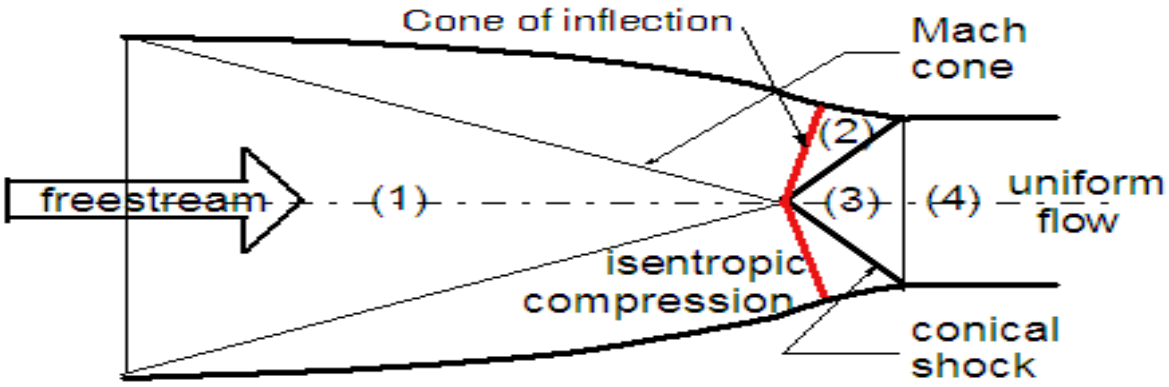


Figure 2.0 Major sections of a typical Busemann flow [8]

A preferred geometry for a scramjet combustor is a circular cross-section duct because of its superior ability to withstand both heat and pressure loads. Frictional losses are also at a minimum for such a duct since a cylinder has the smallest surface area for a given cross-sectional area. This leads to a cylindrical (axially symmetric) geometry as being desirable also for the intake that is attached to the front of the combustor duct. Full Busemann has such a circular cross section.

## 3.0 Busemann Flow Theory *

Taylor-McColl (T-M) equation (1) in its original mode is shown below. Constant property radials in a Busemann Intake calculated based on Taylor-McColl equations is shown in Figure 3.1.

$$\left(1-\frac{v^2}{a^2}\right)\frac{d^2u}{d\theta^2}+\cot\theta\frac{du}{d\theta}+\left(2-\frac{v^2}{a^2}\right)u=0 \qquad v=\frac{du}{d\theta} \tag{1}$$

The most well-known numerical integration of this equation is for the flow over an axisymmetric cone at zero angle of attack in supersonic flow. Taylor-McColl equations (2) and (3) are arranged in terms of the radial and azimuthal Mach numbers (u, v), see Figure. 3.0:

$$\frac{du}{d\theta}=v+\frac{\gamma-1}{2}uv\frac{u+v\cot\theta}{v^2-1} \tag{2}$$

$$\frac{dv}{d\theta}=-u+(1+\frac{\gamma-1}{2}v^2)\frac{u+v\cot\theta}{v^2-1} \tag{3}$$

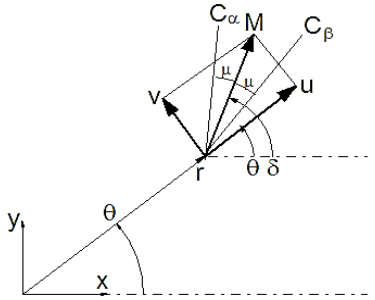


Figure 3.0 Radial and azimuthal Mach numbers (u, v), in equations (2) and (3)

Equations (2) and (3) are integrated - using a standard Runge Kutta method - with respect to $\theta$ from the front of the conical shock (station 2 in Figure 2.0) to the freestream (station 1). Starting values: $u_2$, $v_2$ (equations 4 and 5 respectively) and $\theta_2$ are calculated from the Mach number in front of the shock, $M_2$, and the aerodynamic shock angle, $\theta_{23}$.

$$u_2=M_2\cos\theta_{23} \tag{4}$$

$$v_2=-M_2\sin\theta_{23} \tag{5}$$

*Most formulae and relations used in this section are summarized and edited directly from reference [9] with communicative permission from its author, S. Molder and are presented here for continuity of this report.

The flow deflection through the shock is given by equation (6) [10]:

$$\tan\delta_{12} = \frac{2\cot\theta_{23}\left(M_2^2\sin^2\theta_{23}-1\right)}{2M_2^2\left(\gamma+1-2\sin^2\theta_{23}\right)} \tag{6}$$

The exit Mach number in region (3) of Figure 4.0 is found through equation (7):

$$M_3^2 = \frac{(\gamma+1)^2 M_2^2 k^2 - 4(k^2-1)(\gamma k^2+1)}{[2\gamma k^2-(\gamma-1)][(\gamma-1)k^2+2]} \qquad \text{where} \quad k^2 = M_2^2\sin^2\theta_{23} \tag{7}$$

The T-M streamline equation in spherical coordinates is given by equation (8):

$$dr/d\theta = ru/v \tag{8}$$

Equation (8) is not coupled to (2) or (3), since r does not appear in (2) or (3), so that it could be integrated separately. It is most convenient to integrate equation (8) alongside (2) and (3).

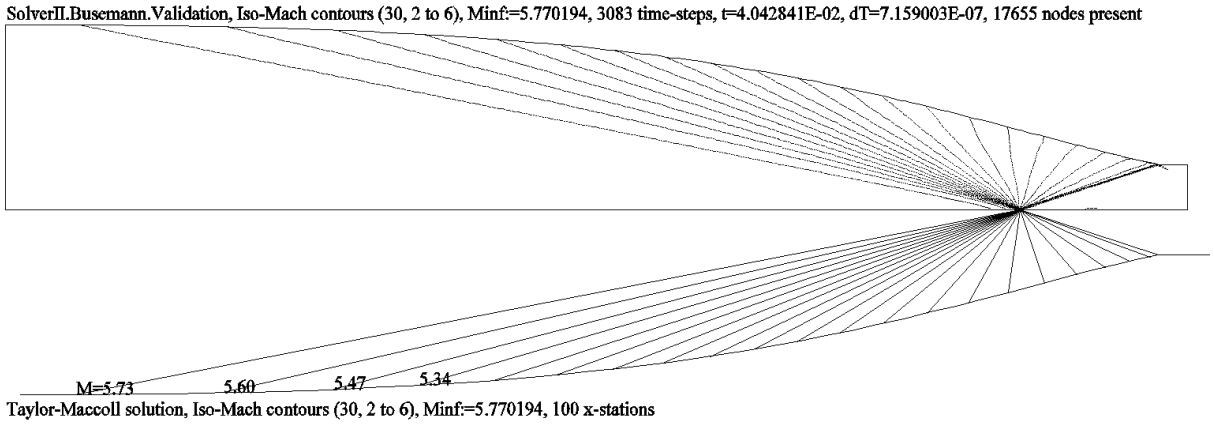


Figure 3.1 Constant property radials in a Busemann Intake [2].

## 4.0 Lens Analogy (LA) Intake

*A uniform, invisid, shock free flow, at a supersonic Mach number M1, can be transformed downstream into a different uniform supersonic flow at a Mach number M2. This type of flow is reversible and therefore M2 may be larger or smaller than M1. When M2 is larger than M1, we have an expansive nozzle like flow with a favorable pressure gradient. When M2 (>1) is less than M1, the flow is compressive, as in a diffuser, and the pressure gradient is an adverse one. Since the cross-sectional area of the stream is expanded (contracted) if M2 > M1 (M1 > M2), the transformation is conceptually analogous to what several lenses can do with an optical beam; hence, the name lens analogy (LA)* [4].

The lens analogy flow consists of joining three simple planar flows in a tandem downstream sequence as shown in Figure 4.0. The two-dimensional LA flow is assumed to be steady, inviscid, shock free and the fluid behaves as a perfect gas.

The flows to the left of the line AA' and to the right of the line BB" are parallel and uniform. Flows in regions enclosed by AA'A" and BB'B" are compressive Prandtl-Meyer flows. In region enclosed by AA"B'B the flow converges towards a line sink [4].

Matching Mach number and flow direction at every location on the lines AA" and BB' yields to an explicit analytical expression for the wall shape A'A"B'B" (equations 9, 10, 11 and 12). The line A"B' is straight and can be any length including zero. For a unit intake height the variables are: gas specific heat ratio (ɣ), M1, M3 and A"B' segment length (dl). Sketch of the lower half of a symmetric two-dimensional LA diffuser is shown in Figure 4.0 and an actual example of a surface generated using ɣ =1.4, M1=3.0 and M2=2.0 is shown in Figure 4.1.

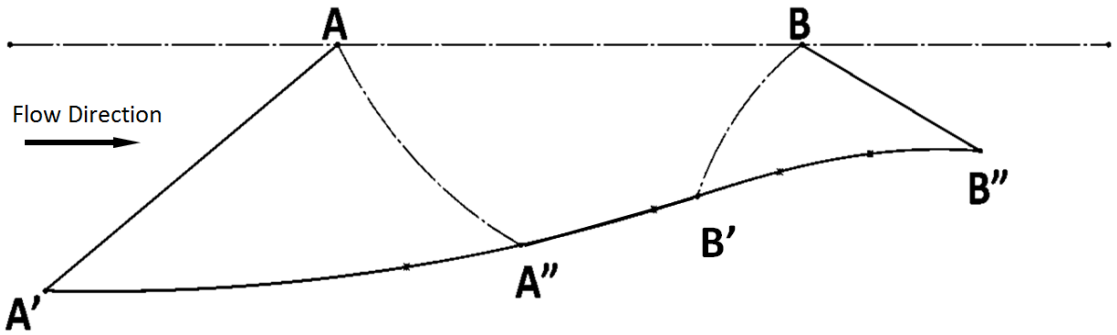


Figure 4.0 Sketch of the lower half of a symmetric two-dimensional LA diffuser.

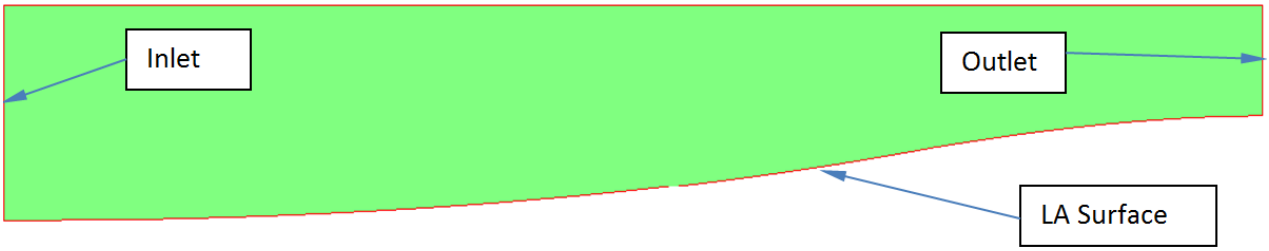


Figure 4.1 Lens Analogy surface generated using ɣ =1.4, M1=3.0, M2=2.0 and dl=0.

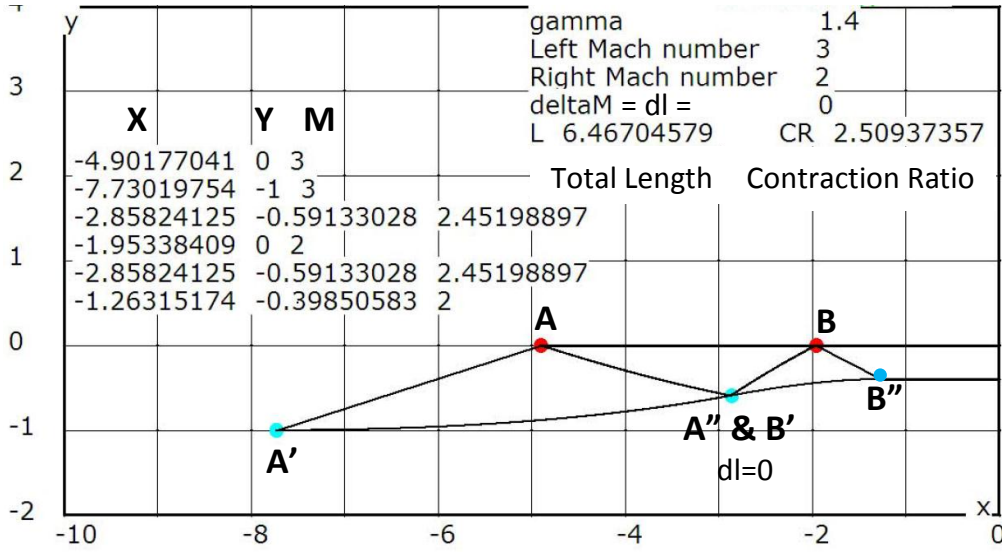


Figure 4.2 AA’A” and BB’B” points on an LA intake for: ɣ =1.4, M1=3.0, M2=2.0 and dl=0.

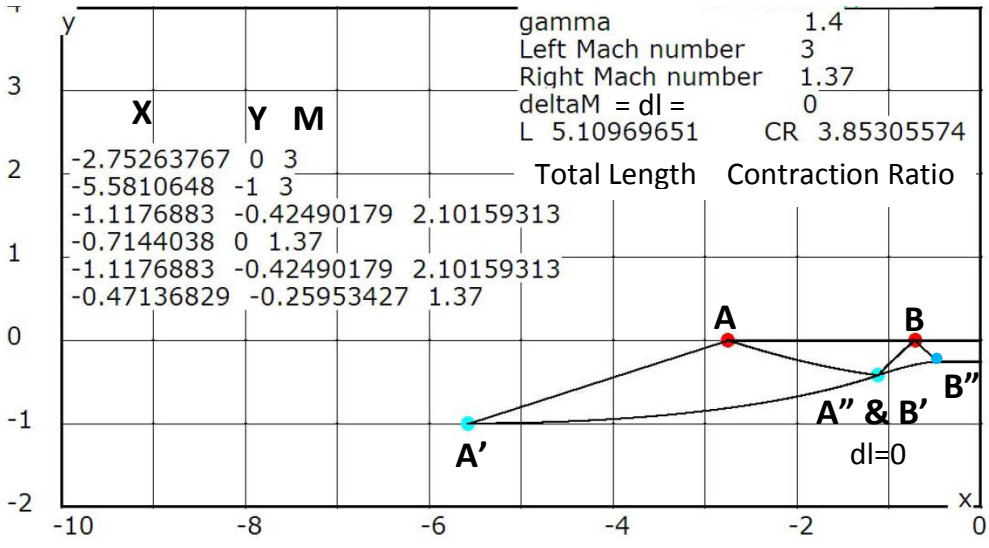


Figure 4.3 AA’A” and BB’B” points on an LA intake for: ɣ =1.4, M1=3.0, M2=1.37 and dl=0.

Figure 4.1 is generated for: ɣ =1.4, M1=3.0, M2=2.0 and dl=0, using Emanuel's LA formulation (equations 9, 10, 11 and 12) incorporated into a Microsoft Excel program. Full content of the relationships used in the excel program is found in reference [4]. In all cases, since dl=0, points A" and B' coincide.

Figures 4.2 and 4.3 illustrate an LA case generated for: ɣ =1.4, M1=3.0, M2=2.0, dl=0 and ɣ =1.4, M1=3.0, M2=1.37, dl=0, respectively using Molder's QBasic program and the two methods agreed within 0.017%. The x, y coordinates (equations 13 through 21) and Mach number for points (AA'A" and BB'B") are given on the graph. In addition Mach number at each point, the intake total length, and compression ratio values are found on the graph.

Explicit analytical expressions (x, y coordinates) for the wall shape A'A" is given by (9) and (10).

$$x = -\frac{1}{\phi}\frac{M_1}{M}\left(\frac{X}{X_1}\right)^{(\gamma+1)/[2(\gamma-1)]}\left\{\cos\theta + (\phi-\theta)\left[(M^2-1)^{1/2}\cos\theta - \sin\theta\right]\right\} \quad (9)$$

$$y = -\frac{1}{\phi}\frac{M_1}{M}\left(\frac{X}{X_1}\right)^{(\gamma+1)/[2(\gamma-1)]}\left\{\sin\theta + (\phi-\theta)\left[(M^2-1)^{1/2}\sin\theta + \cos\theta\right]\right\} \quad (10)$$

Explicit analytical expressions (x, y coordinates) for the wall shape B'B" is given by (11) and (12).

$$x = \frac{1}{\phi}\frac{M_1}{M}\left(\frac{X}{X_1}\right)^{(\gamma+1)/[2(\gamma-1)]}\left\{-\cos\theta + (\phi-\theta)\left[\sin\theta + (M^2-1)^{1/2}\cos\theta\right]\right\} \quad (11)$$

$$y = \frac{1}{\phi}\frac{M_1}{M}\left(\frac{X}{X_1}\right)^{(\gamma+1)/[2(\gamma-1)]}\left\{\sin\theta + (\phi-\theta)\left[\cos\theta - (M^2-1)^{1/2}\sin\theta\right]\right\} \quad (12)$$

Equations to calculate x, y coordinates for A, A', A", B, B', and B" are given by (13) through (21).

$$x_A = -\frac{R^*}{M_1}\left(\frac{2}{\gamma+1}X_1\right)^{(\gamma+1)/[2(\gamma-1)]}, \quad y_A = 0 \quad (13)$$

$$x_B = -\frac{R^*}{M_2}\left(\frac{2}{\gamma+1}X_2\right)^{(\gamma+1)/[2(\gamma-1)]}, \quad y_B = 0 \quad (14)$$

$$x_{A'} = x_A - (M_1^2-1)^{1/2}, \quad y_{A'} = -1 \quad (15)$$

$$x_{B'} = -\frac{\cos\phi}{\phi}\frac{M_1}{M_B}\left(\frac{X_{B'}}{X_1}\right)^{(\gamma+1)/[2(\gamma-1)]} \quad (16) \qquad y_{B'} = x_{B'}\tan\phi \quad (17)$$

$$x_{A''} = -\frac{\cos\phi}{\phi}\frac{M_1}{M_{A''}}\left(\frac{X_{A''}}{X_1}\right)^{(\gamma+1)/[2(\gamma-1)]} \quad (18) \qquad y_{A''} = x_{A''}\tan\phi \quad (19)$$

$$x_{B''} = x_B - y_{B''}(M_2^2-1)^{1/2} \quad (20) \qquad y_{B''} = -\frac{M_1}{M_2}\left(\frac{X_2}{X_1}\right)^{(\gamma+1)/[2(\gamma-1)]} \quad (21)$$

## 5.0 Limit Lines

Emanuel has shown that below an exit Mach number of 1.37 there exists a singularity or limit line in the streamline shape. A streamline arriving at the limit line reverses direction by $180^{o}$ to flow in the opposite (upstream) direction at the exit plane.

Although predicted by analysis, such flow behaviour does not seem physically possible because the flow would have to somehow penetrate itself. However the question still arises as to what happens to the actual flow on the contour of this analytically predicted line. Why does the analytical method fail to produce a continued realistic contour? What would happen experimentally? Does a shockwave occur?

Figure 5.0 shows limit line according to Emanuel and Figures 5.1a-b show same location on a numerically generated surface.

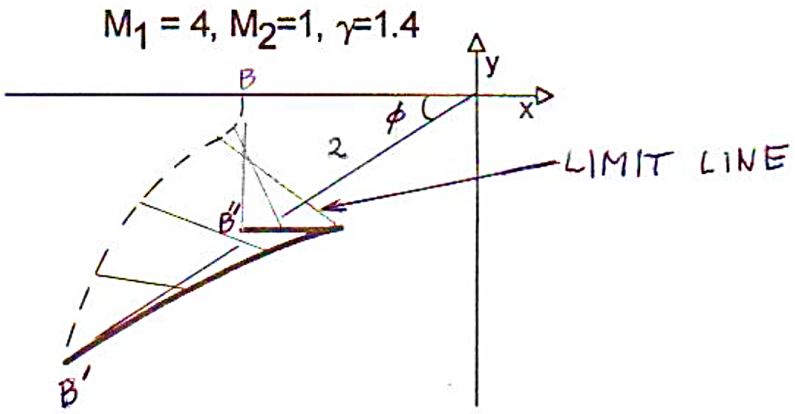


Figure 5.0 limit line on an LA intake for M1=4.0, M2=1.0 and ɣ =1.4. ref. [4]

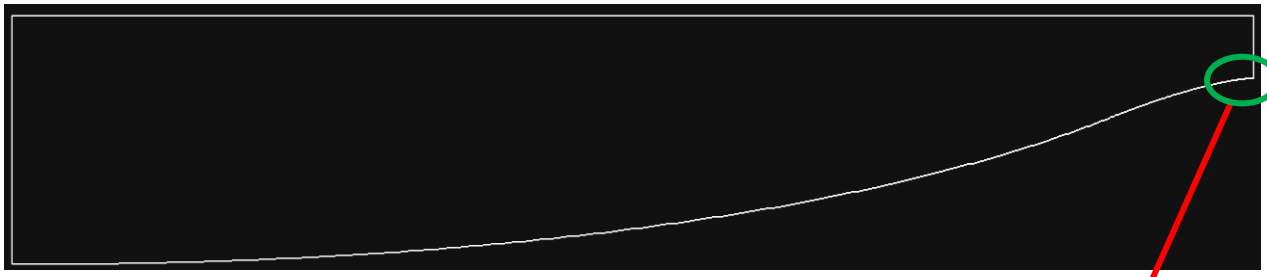

Figure 5.1a LA for: ɣ =1.4, M1=3.0, M2=1.3 and dl=0 (flow left to right)

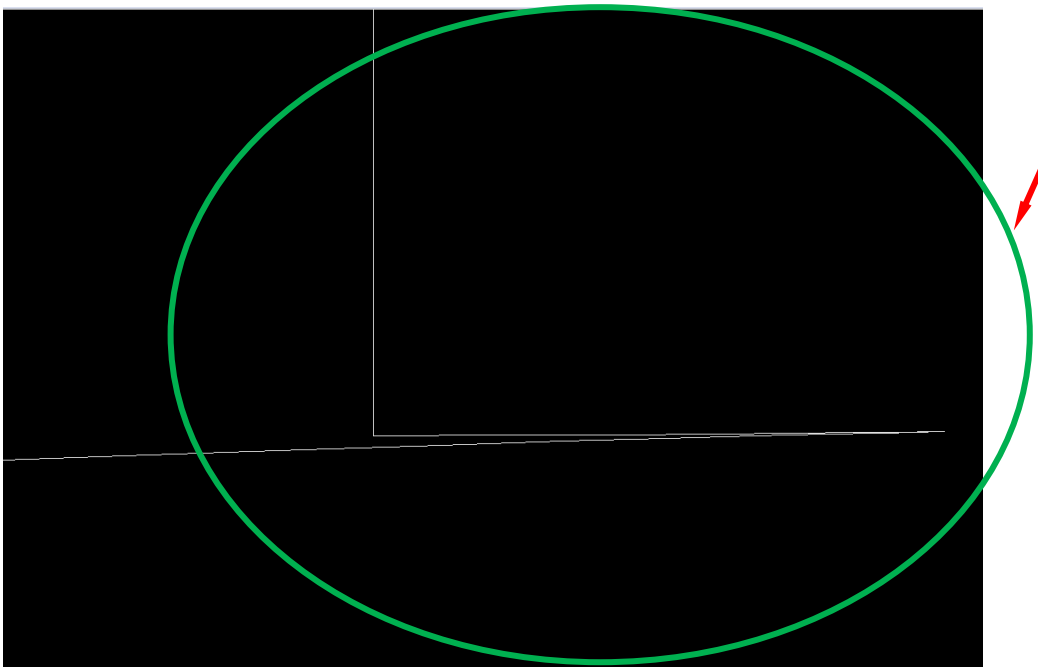

Figure 5.1b Close up of the exit corner

200 points were generated for B'B" section (Figure 4.0) and a reversal was noticed at the exit corner. As is shown (boxed) the last eight numbers reverse their direction both in x and y axis.

| X | Y |
|---|---|
| -.4516236 | -.2518032 |
| -.451586 | -.2518025 |
| -.4515778 | -.2518023 |
| -.4515994 | -.2518027 |
| -.4516505 | -.2518034 |
| -.4517313 | -.2518043 |
| -.4518419 | -.2518054 |
| -.4519824 | -.2518066 |
| -.452153 | -.2518077 |
| -.4523536 | -.2518086 |
| -.4525844 | -.2518092 |

| | X | Y | M |
|---|---|---|---|
| A | -2.62902698 | 0 | 3 |
| A' | -5.45745411 | -1 | 3 |
| A" | -1.02896967 | -0.41142374 | 2.06653333 |
| B | -0.66201403 | 0 | 1.3 |
| B' | -1.02896967 | -0.41142374 | 2.06653333 |
| B" | -0.45284533 | -0.25180952 | 1.3 |

AA'A" and BB'B" points and Mach numbers (see Figure 4.3)

## 6.0 Busemann vs. Lens Analogy (LA) Intakes.

It is important to compare similarities and differences between intake type flows generated by those two methods.

Both methods:

a) Transform a uniform and parallel supersonic / hypersonic flow to a lower uniform and parallel flow.
b) Both methods depend on using a constant value of gas specific heat ratios: ɣ.

The flows differ by:

a) Busemann flow is axial. Lens Analogy (LA) flow is planar.
b) Busemann flow is also conically symmetric. LA flow has no such additional symmetry.
c) LA flow is isentropic, hence reversible. It can be used to generate nozzle contours as well as intake contours. Busemann flow, because of the trailing shock, is irreversible and can be used to generate intake flows only.
d) Busemann intake shapes are found numerically from the (Runge-Kutta) integration of a second order Total Differential Equation (The Taylor-McColl equation(s)). No explicit solution exists. The planar LA flow and contour are given by explicit expressions.
e) The LA flow definition has one extra variable, the sink-flow length section from A" to B' (dl). This makes it possible to vary the length of the LA. Such variation could be useful to decrease the adverse pressure gradient thereby alleviating boundary layer separation problem. A similar decrease in pressure gradient for the Busemann intake could be attained only by increasing the overall size of the intake.

It is noted that LA is applicable also to axial flows. Such axial flows would be more closely comparable to Busemann flows. The axial flow version involves the use of the Method of Characteristics (MOC). It no longer yields explicit solutions and its application is much more complicated than for planar flow [4].

The study of the axial flow LA is left for a future project.

## 7.0 The FVM-based CFD Code (SOLVER II) grid file

Work reported herein has been carried out using SOLVER II, an unstructured, time-dependent, solution-adaptive, multi-block, MUSCL-type, Euler code. A numerical method utilizing these features should provide reliable results, so long as the flows being studied are devoid of large zones of separated flow.

First and last pages of the grid file for CFD code (SOLVER II) is shown below. This file, containing (x, y) coordinates of the surface points, is required as input to the code that generates the computational grid for the SLOVER II CFD code. It is generated using equations (9) through (21).

First page of the grid file is shown below where mesh parameters are set.

```
1e-6  minimal_radius                          !  g      s     g   f  a  b
1e+6  maximal_radius                          !   l   l   e   n s   o  l  l   s
1.6   aspect_ration                           !    o a     t i       r  l  o k
0.3   grid_roughness                          !     b       t             c

0  0  1E-3   1.771  1.6   1    block_settings ! x,y,Rmin,Rmax,asp.ratio,block number
*0   0  1E-3   1E3    1.6   2    block_settings ! x,y,Rmin,Rmax,asp.ratio,block number

*autodotting_off                             ! useful feature for some applications
distribution_function                         ! useful feature for some applications
fine_smoothing                                ! more fine smoothing than usual
*binary_output                                ! intermediate binary output (.~2s)
*eps_output                                   ! PostScript output (.eps)
*plt_output                                   ! HPGL output (.plt) (to be viewed by grapher's view.exe)
*dxf_output                                   ! AutoCAD output (.dxf)
```

| *x1 | y1 | x2 | y2 | arc | grid step | bndnumber | line(1)/circle(2) |
|---|---|---|---|---|---|---|---|
| -5.5810650 | -1.0000000 | -5.5392680 | -0.9999683 | 0 | 0.1 | 1 | 1 |
| -5.5392680 | -0.9999683 | -5.4977450 | -0.9998741 | 0 | 0.1 | 1 | 1 |
| -5.4977450 | -0.9998741 | -5.4564880 | -0.9997174 | 0 | 0.1 | 1 | 1 |
| -5.4564880 | -0.9997174 | -5.4154980 | -0.9995001 | 0 | 0.1 | 1 | 1 |
| -5.4154980 | -0.9995001 | -5.3747740 | -0.9992217 | 0 | 0.1 | 1 | 1 |
| -5.3747740 | -0.9992217 | -5.3343130 | -0.9988835 | 0 | 0.1 | 1 | 1 |
| -5.3343130 | -0.9988835 | -5.2941160 | -0.9984862 | 0 | 0.1 | 1 | 1 |
| -5.2941160 | -0.9984862 | -5.2541800 | -0.9980299 | 0 | 0.1 | 1 | 1 |
| -5.2541800 | -0.9980299 | -5.2145050 | -0.9975164 | 0 | 0.1 | 1 | 1 |

Last Page of the grid file is shown below where boundary conditions are set.

| | | | | | | | |
|---|---|---|---|---|---|---|---|
| -0.4743181 | -0.2595653 | -0.4739000 | -0.2595580 | 0 | 0.1 | 1 | 1 |
| -0.4739000 | -0.2595580 | -0.4735091 | -0.2595520 | 0 | 0.1 | 1 | 1 |
| -0.4735091 | -0.2595520 | -0.4731457 | -0.2595470 | 0 | 0.1 | 1 | 1 |
| -0.4731457 | -0.2595470 | -0.4728096 | -0.2595430 | 0 | 0.1 | 1 | 1 |
| -0.4728096 | -0.2595430 | -0.4725009 | -0.2595399 | 0 | 0.1 | 1 | 1 |
| -0.4725009 | -0.2595399 | -0.4722194 | -0.2595376 | 0 | 0.1 | 1 | 1 |
| -0.4722194 | -0.2595376 | -0.4719656 | -0.2595360 | 0 | 0.1 | 1 | 1 |
| -0.4719656 | -0.2595360 | -0.4717390 | -0.2595349 | 0 | 0.1 | 1 | 1 |
| -0.4717390 | -0.2595349 | -0.4715399 | -0.2595344 | 0 | 0.1 | 1 | 1 |
| -0.4715399 | -0.2595344 | -0.4713682 | -0.2595342 | 0 | 0.1 | 1 | 1 |
| -0.4713682 | -0.2595342 | -0.4713682 | 0.0000000 | 0 | 0.1 | 4 | 1 |
| -0.4713682 | 0.0000000 | -5.5810650 | 0.0000000 | 0 | 0.1 | 1 | 1 |
| -5.5810650 | 0.0000000 | -5.5810650 | -1.0000000 | 0 | 0.1 | 6 | 1 |

## 8.0 CFD Code verification

A CFD (SOLVER II) code is used to calculate the flow inside a Busemann intake as predicted by Taylor-McColl equation(s). This will serve to verify the capability of the CFD (SOLVER II) code to simulate an "exact" conical flow.

A Busemann surface for freestream Mach number, M1=8.336 and ɣ =1.4 was generated using Molder's QBasic program (see Appendix B). Coordinates were incorporated into the FVM-based SOLVER II and solutions were obtained. Figures 8.0 to 8.5 show the settings and results obtained. A brief discussion of each illustration follows each Figure.

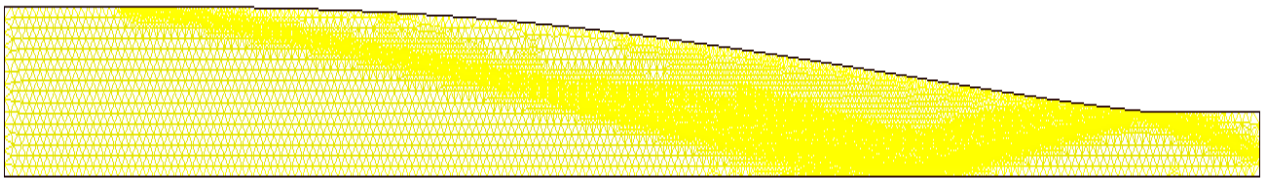

Figure 8.0 Busemann half surface and mesh for freestream Mach number, M1=8.336

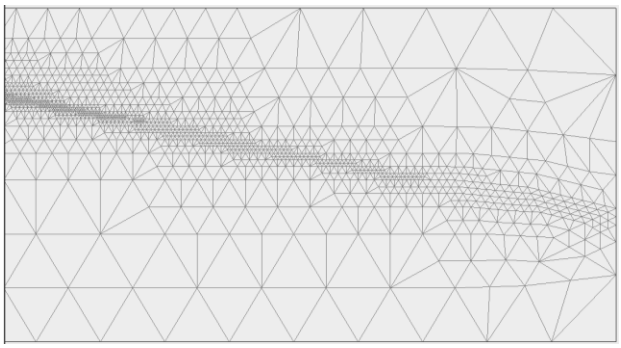

Figure 8.1 A close up of refined mesh regions. Automatic grid refinement is apparent in regions of high flow gradients.

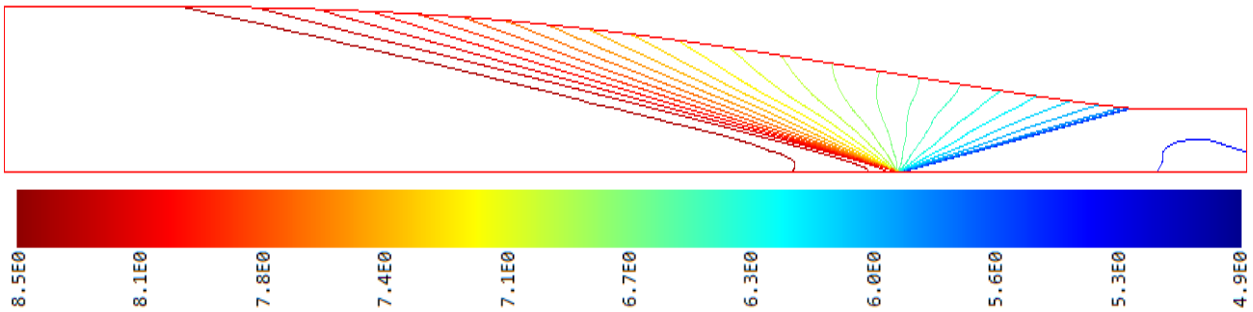


Figure 8.2 Constant Mach number contours and the scale bar for Mach number, M1=8.336

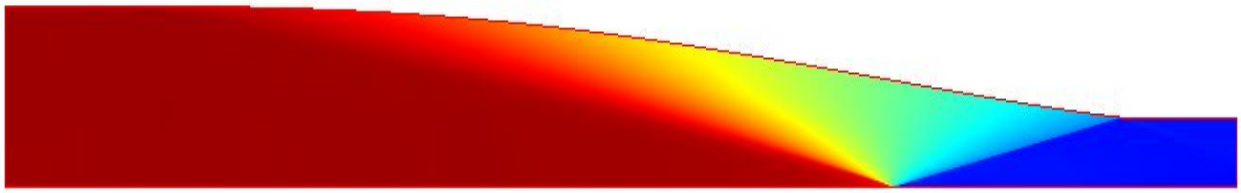

Figure 8.3 Mach number contours for Mach number, M1=8.336

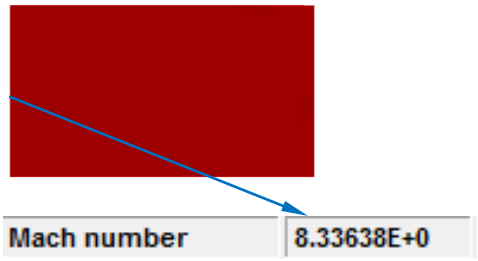


Figure 8.4 Freestream Mach number (M8.336)

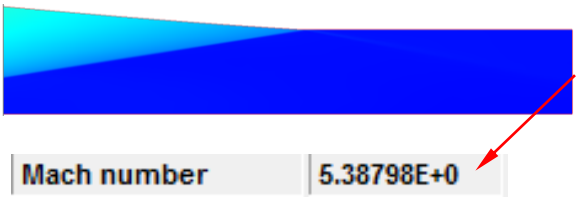


Figure 8.5 Exit Mach number (M5.39)

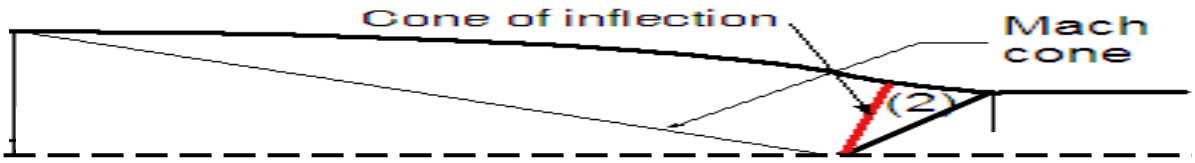


Lower half of Figure 2.0 (reference)

A comparison is shown of the analytical T-M solution and CFD (SOLVER II) results. Visual inspection of Figures 8.2 and 8.3 shows that CFD solution is predicting a conically symmetric flow.

## 9.0 CFD Results

Total of 6 cases have been run and results are examined. Table 1.0 shows a summary for these cases. Cases 5 and 6 are run in search of the limit line predicated by Emanuel.

Table 1.0 Summary of CFD Cases

| | | Taylor-McColl Design | | CFD | |
|---|---|---|---|---|---|
| Case # | Intake Type | Inlet Design Mach Number | Exit Design Mach Number | Freestream Mach Number | Calculated Exit Mach Number |
| 1 | Busemann | 8.336 | 5.40 | 8.336 | 5.388 |
| 2 | Lens Analogy LA) | 3.0 | 2.0 | 3.0 | 1.99915 |
| 3 | Lens Analogy LA) | 7.0 | 4.0 | 6.99406 | 3.96301 |
| 4 | Lens Analogy LA) | 7.0 | 4.0 | 6.0* | 3.29769 |
| 5 | Lens Analogy LA) | 3.0 | 1.37 | 3.0 | 1.34 |
| 6 | Lens Analogy LA) | 3.0 | 1.3 | 3.00019 | 1.64593 |

* Note: Off-Design Mach number (M6) from the Mach 7 – Mach4 LA contour.

Snapshot of the results for each case are presented and a brief note is included for each Figure.

Case #1's results (Busemann with M1=8.336) have been presented earlier in section 8.0 (CFD Code verification).

Case #2: Figures 9.0 to 9.4 show CFD result snapshots for: **ɣ =1.4, M1=3.0, M2=2.0 and dl=0**, using Emanuel's formulation and CFD code (SOLVER II).

**Opening Points at A'**

| | |
|---|---|
| -7.7301980 | -1.0000000 |
| -7.6934780 | -0.9999830 |
| -7.6569120 | -0.9999324 |
| -7.6204960 | -0.9998484 |
| -7.5842300 | -0.9997309 |

**Closing Points at B"**

| | |
|---|---|
| -1.2723650 | -0.3985158 |
| -1.2677390 | -0.3985083 |
| -1.2677390 | 0.0000000 |
| -7.7301980 | 0.0000000 |

**M1=3.0, M2=2.0, Gamma=1.4**

```
[Scales]
r_sc=1.225
p_sc=101325.
L_sc=0.1
Rgas_sc=8314.
u_sc=sqrt(p_sc/r_sc)
t_sc=L_sc/u_sc
a_sc=L_sc/t_sc^2
```

```
[GasDynam]
McNum=3.0
ShowGasErrors=0
InterfaceDiag=0
InterfaceCorr=1
MaxBTypes=32
MaxSpecies=2

GasGamma(01)=1.4
GasMolWt(01)=28.97 '//air

GasGamma(02)=1.4
GasMolWt(02)=28.97 '//air

CFLnum=0.7  '// 0.7
```

Total of 400 points was generated for the LA surface from A' to B" (see Figure 4.0). First and last few x - y coordinates are shown above along with gas dynamic constant settings. Note that x – y values have been normalized with respect to the inlet height.

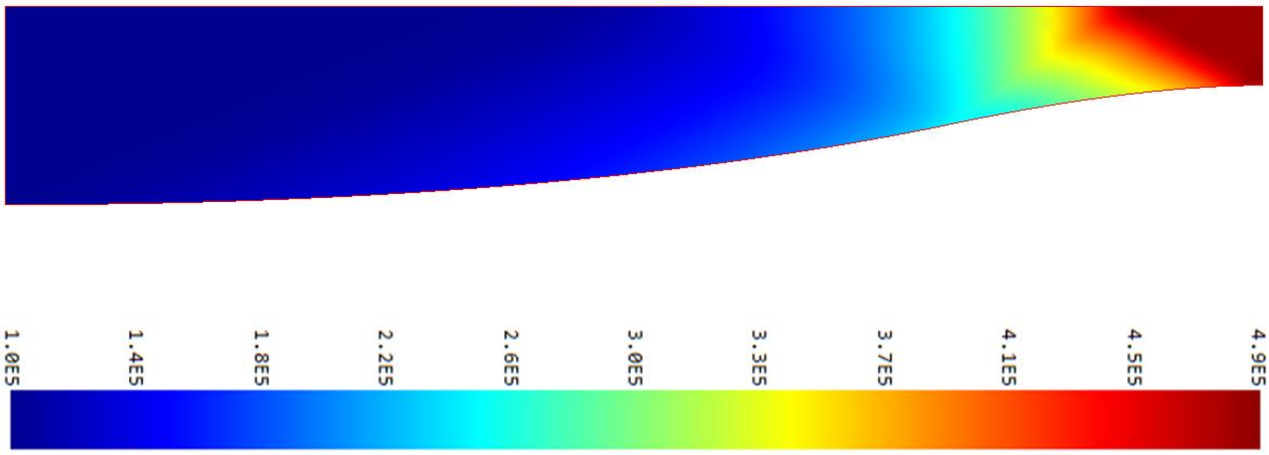


Figure 9.0 pressure contours and scale bar in kPa.

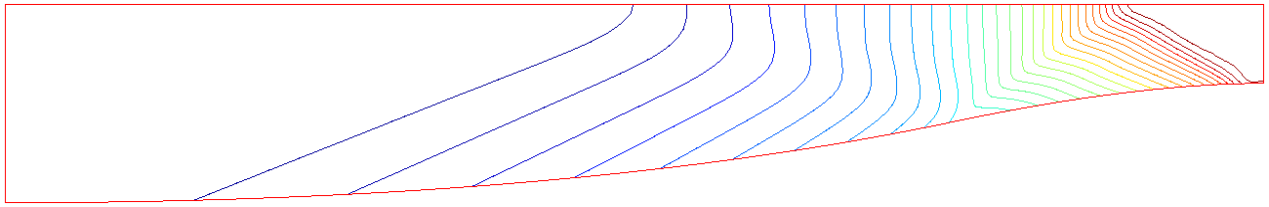

Figure 9.1 constant pressure contours (Isobars)

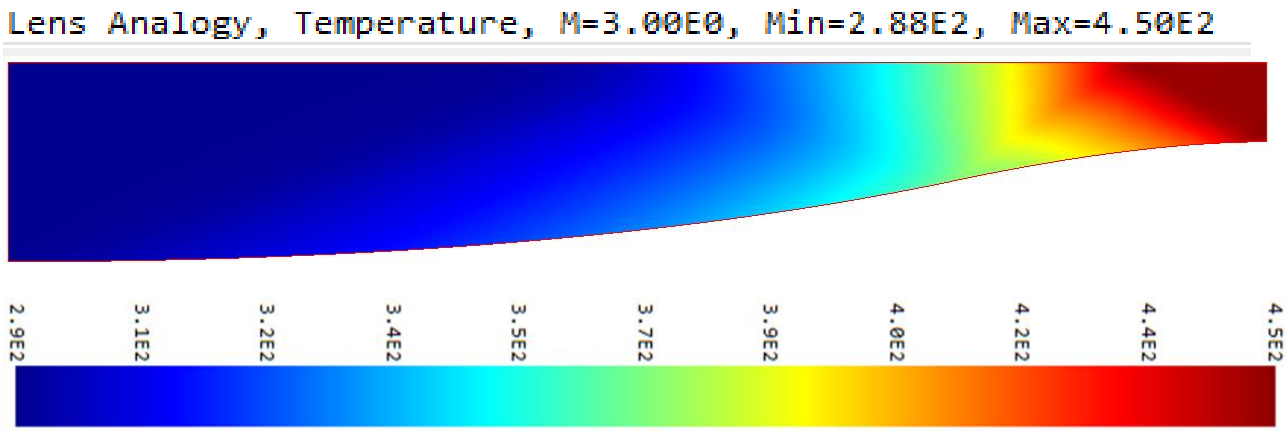


Figure 9.2 temperature contours and scale bar with minimum of 288 k and maximum of 450 k.

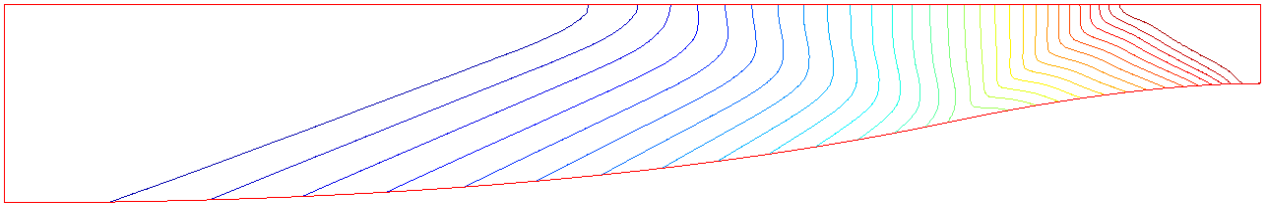

Figure 9.3 constant temperature contours

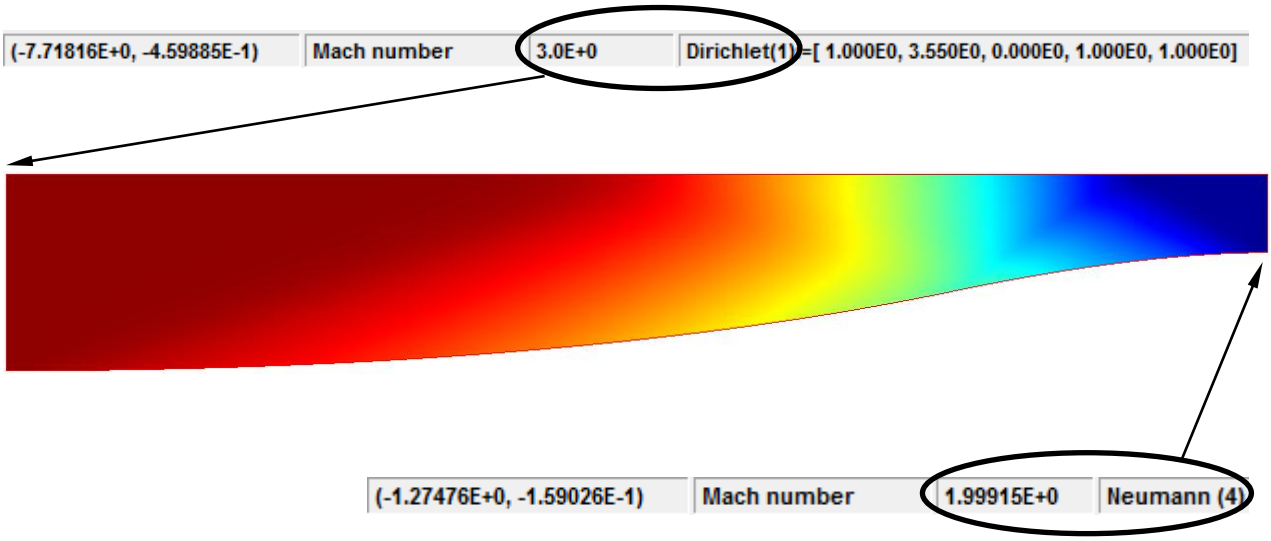


Figure 9.4 Shows inlet boundary and exit types and Mach numbers.

A visual inspection of the results above indicates that no shockwave is present in the flow.

Case #3: Figures 9.5 to 9. 9 show CFD result snapshots for: **ɣ =1.4, M1=7.0, M2=4.0 and dl=0**, using Emanuel's formulation and CFD code (SOLVER II) at design Mach number of 7.0.

```
[GasDynam]
McNum=7.0
ShowGasErrors=0
InterfaceDiag=0
InterfaceCorr=1
MaxBTypes=32
MaxSpecies=2

GasGamma(01)=1.4
GasMolWt(01)=28.97 '//air

GasGamma(02)=1.4
GasMolWt(02)=28.97 '//air

CFLnum=0.7  '// 0.7
```

| *x1 | y1 | | |
|---|---|---|---|
| -11.4776695 | -1.0000000 | -0.0800758 | -0.1029587 |
| -11.3742877 | -0.9999564 | -0.0779384 | -0.1029459 |
| -11.2716587 | -0.9998265 | -0.0758249 | -0.1029360 |
| -11.1697783 | -0.9996111 | -0.0737351 | -0.1029290 |
| -11.0686423 | -0.9993115 | -0.0716688 | -0.1029249 |
| -10.9682465 | -0.9989286 | -0.0696260 | -0.1029235 |
| -10.8685865 | -0.9984635 | -0.0696260 | 0.0000000 |
| -10.7696583 | -0.9979171 | -11.4776695 | 0.0000000 |

Total of 400 points were generated for the LA surface from A' to B" (see Figure 4.0). First and last few x - y coordinates are shown above along with gas dynamic constant settings. Note that x – y values have been normalized with respect to the inlet height.

For this case two intermediate time steps are shown to give an indication of its development. The rest are final results after 1550000 time steps.

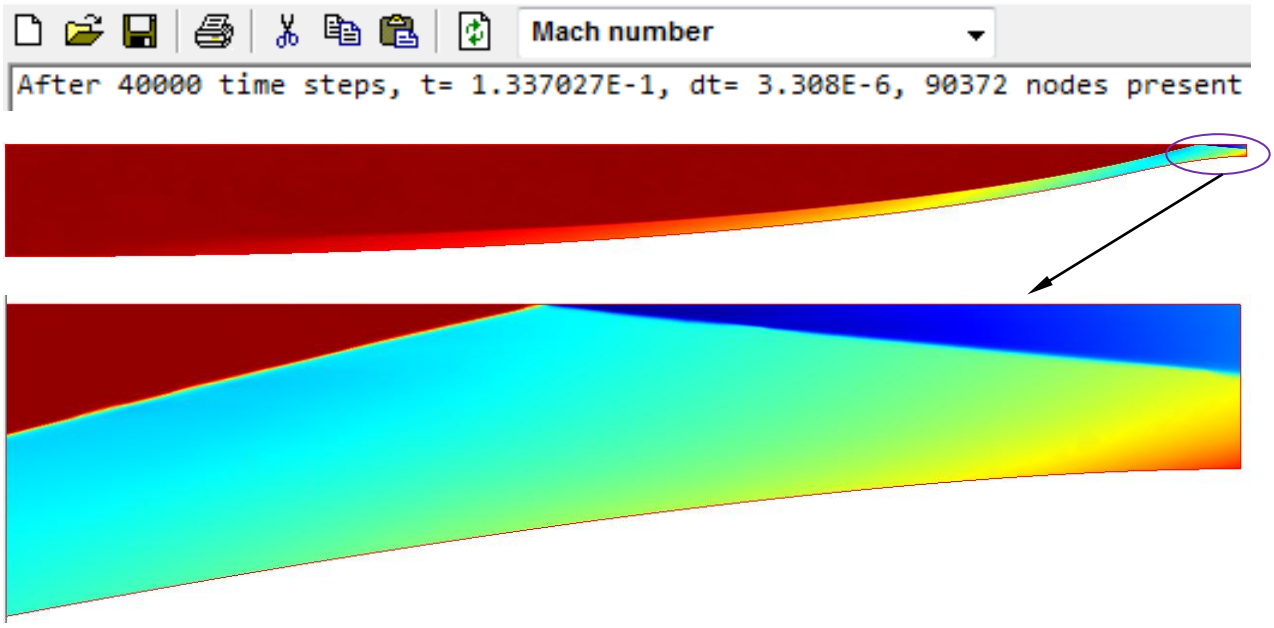


Figure 9.5 shows an intermediate time step (40000 time steps) and a close up.

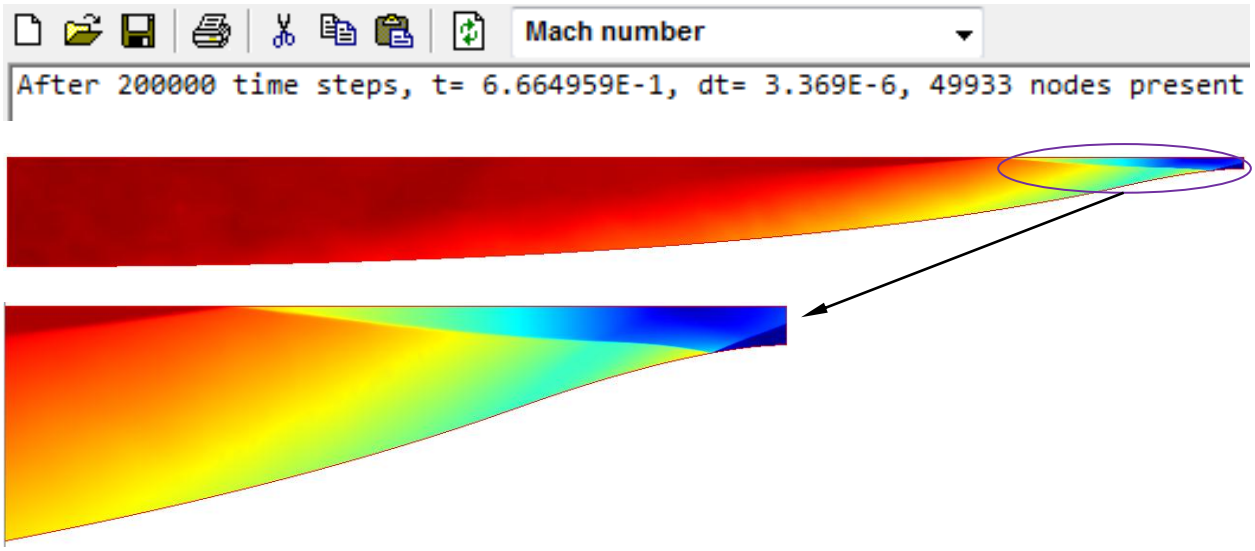


Figure 9.6 shows an intermediate time step (200000 time steps) and a close up.

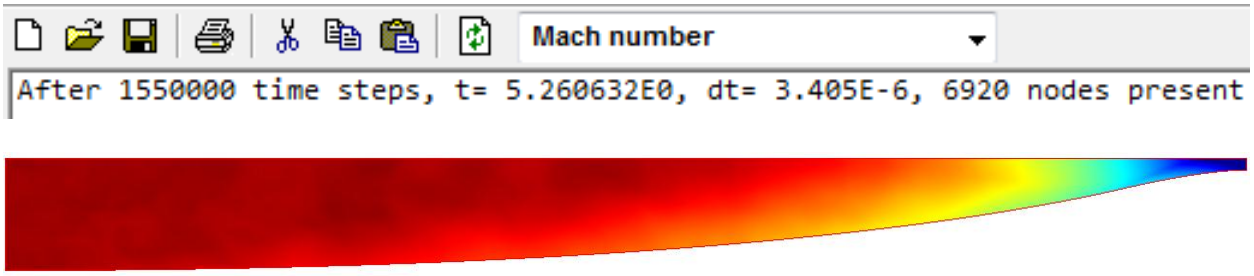


Figure 9.7 shows final filled Mach number contours (1550000 time steps).

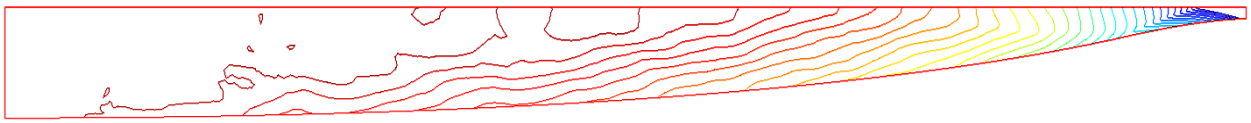

Figure 9.8 shows final constant Mach number contours.


Figure 9.9 Shows inlet, boundary and exit types and Mach numbers.

Case #4: Figures 9.10 to 9.12 show CFD result snapshots for: **ɣ =1.4, M1=7.0, M2=4.0 and dl=0**, using Emanuel's formulation and CFD code (SOLVER II) at off-design Mach number of 6.0.

Figure 9.10 shows final filled Mach number contours (1600000 time steps).

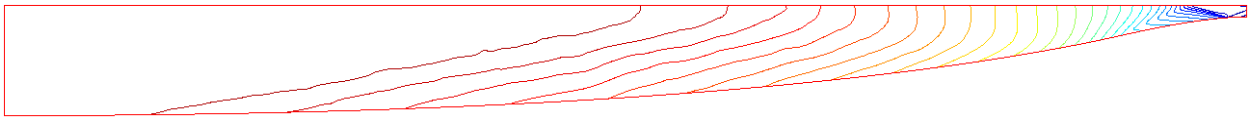

Figure 9.11 shows final constant Mach number contours.

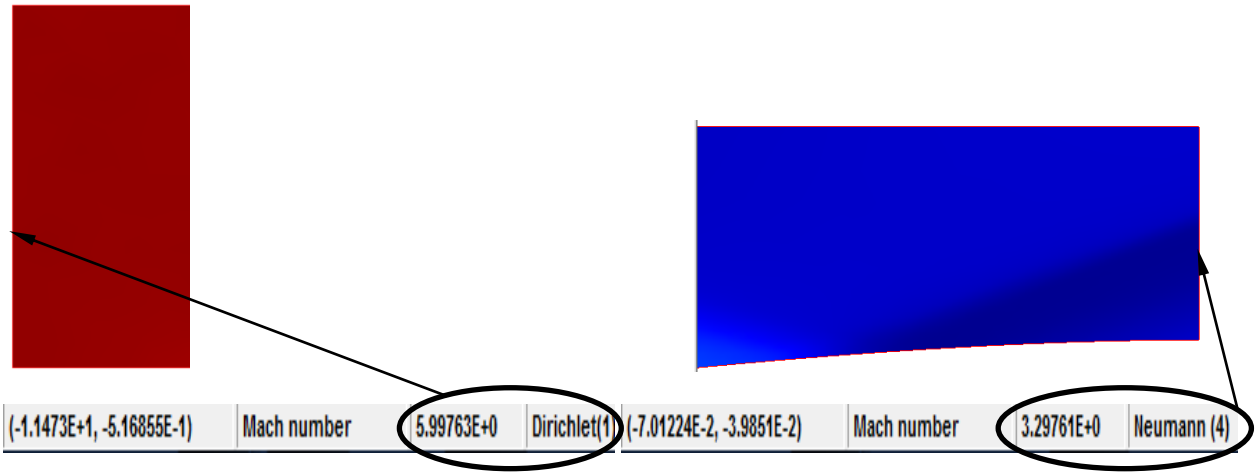


Figure 9.12 Shows inlet, boundary and exit types and Mach numbers.

Case #5: Figures 9.13 and 9.14 show CFD result snapshots for: **γ =1.4, M1=3.0, M2=1.37 and dl=0**, using Emanuel's formulation and CFD code (SOLVER II) at design Mach number of 3.0.

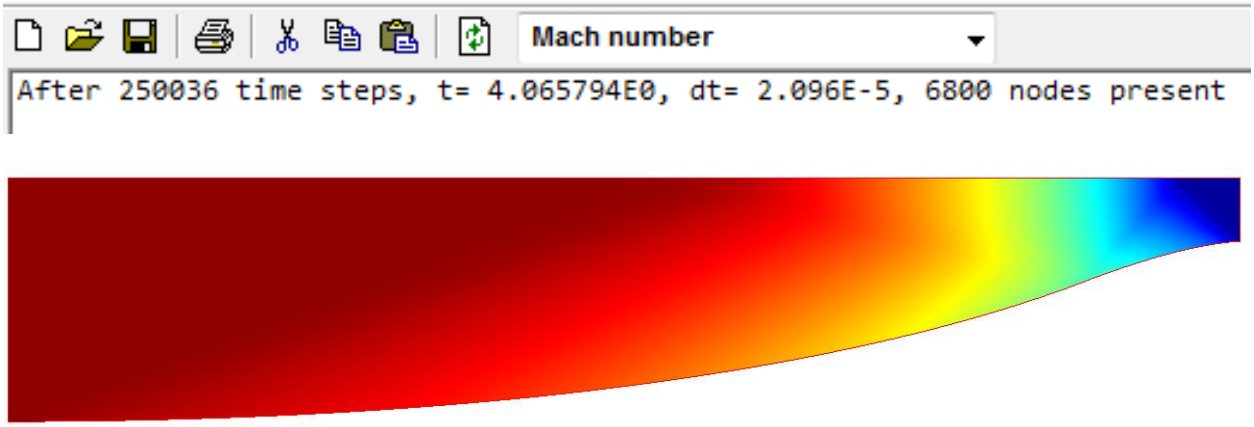


Figure 9.13 shows final filled Mach number contours (250036 time steps).

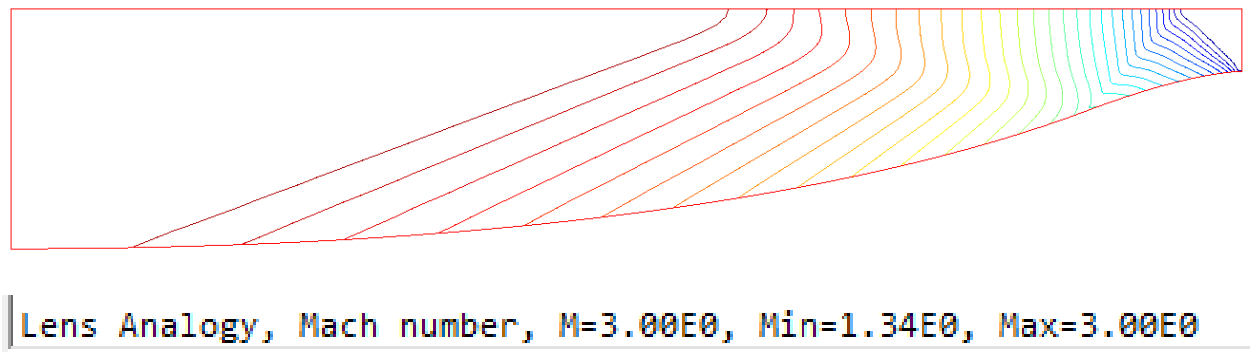


Figure 9.14 shows final constant Mach number contours

Case #6: Figures 9.15 and 9.16 show CFD result snapshots for: **ɣ =1.4, M1=3.0, M2=1.3 and dl=0**, using Emanuel's formulation and CFD code (SOLVER II) at design Mach number of 3.0.

Figure 9.15 shows an intermediate filled Mach number contours (200000 time steps)

Figure 9.16 shows final filled Mach number contours (800000 time steps).

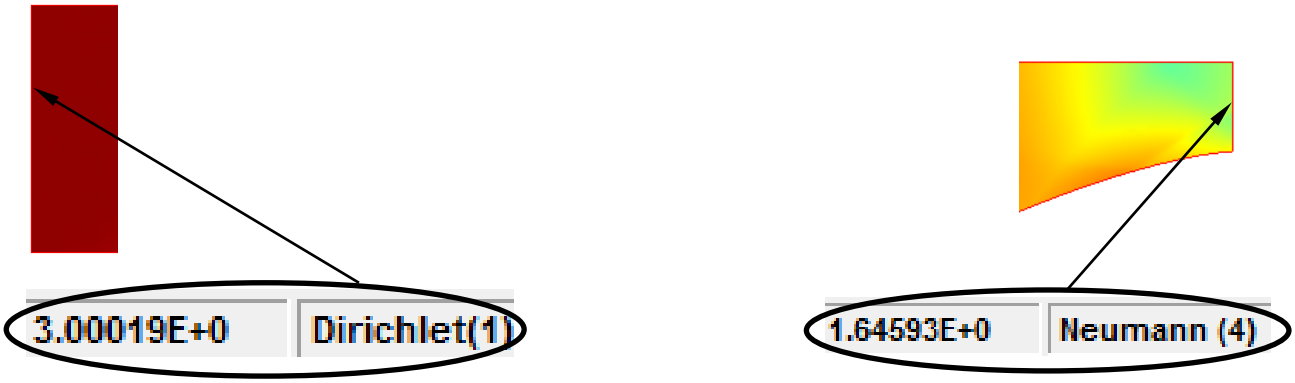


Figure 9.17 Shows inlet, boundary and exit types and Mach numbers.

No limit line is detectable from visual inspection of cases 5 and 6.

## 10.0 Conclusion

The Solver II CFD code calculates results for hypersonic internal flow that appear to correspond to "exact" flow calculated from the Taylor-McColl equations for conically symmetric flow. Numerical values of flow variable agree according to the following table.

Table 2.0 T-M and CFD Comparison

| Case # | Exit Design Mach Number | Freestream Mach Number | Calculated Exit Mach Number | % Difference |
|---|---|---|---|---|
| 1 | 5.40 | 8.336 | 5.388 | 0.2222 |
| 2 | 2.0 | 3.0 | 1.99915 | 0.0425 |
| 3 | 4.0 | 6.99406 | 3.96301 | 0.9247 |
| 4 | 4.0 | 6.0* | 3.29769 | 17.55 |
| 5 | 1.37 | 3.0 | 1.34 (Min) | 2.189 |
| 6 | 1.3 | 3.00019 | 1.64593 | 26.61 |

Contours and flow generated by the Lens Analogy is reproduced and verified by CFD calculations.

The limit line predicted by the Lens Analogy does not appear in CFD calculations.

## 11.0 Future Work

This work should be extended to:

a) Calculate axisymmetric versions of the LA-type intake;

b) Verify the axisymmetric LA contours and flow by CFD calculations;

c) Compare axisymmetric La contours with corresponding Busemann contours and their performance as hypersonic intakes;

d) Further investigate implications of limit lines on the generation of LA contours;

e) Carry out further studies of off-design performance and startability of LA type intakes.

## Appendix A

Emanuel's formulation of LA boundaries including equations (13) to (21) (AA'A" & BB'B") [4]

$$M_A = M_{A'} = M_1, \qquad M_B = M_{B''} = M_2, \qquad \delta M = M_{A''} - M_{B'}$$

$$\nu(M_{B'}) + \nu(M_{B'} + \delta M) = \nu_1 + \nu_2$$

$$M_{A''} = \delta M + M_{B'}$$

$$\phi = \nu_1 - \nu_{A''}$$

$$x_A = -\frac{1}{\phi}, \qquad y_A = 0$$

$$x_B = -\frac{1}{\phi}\frac{M_1}{M_2}\left(\frac{X_2}{X_1}\right)^{(\gamma+1)/[2(\gamma-1)]}, \qquad y_B = 0$$

$$x_{A'} = x_A - (M_1^2 - 1)^{1/2}, \qquad y_{A'} = -1$$

$$x_{A''} = -\frac{\cos\phi}{\phi}\frac{M_1}{M_{A''}}\left(\frac{X_{A''}}{X_1}\right)^{(\gamma+1)/[2(\gamma-1)]}, \qquad y_{A''} = x_{A''}\tan\phi$$

$$x_{B'} = -\frac{\cos\phi}{\phi}\frac{M_1}{M_B}\left(\frac{X_{B'}}{X_1}\right)^{(\gamma+1)/[2(\gamma-1)]}, \qquad y_{B'} = x_{B'}\tan\phi$$

$$y_{B''} = -\frac{M_1}{M_2}\left(\frac{X_2}{X_1}\right)^{(\gamma+1)/[2(\gamma-1)]}$$

$$x_{B''} = x_B - y_{B''}(M_2^2 - 1)^{1/2}$$

$$L = -(x_{A'} - x_{B''})$$

$$= \frac{1}{\nu_1 - \nu_{A''}}\left[1 - \frac{M_1}{M_2}\left(\frac{X_2}{X_1}\right)^{(\gamma+1)/[2(\gamma-1)]}\right] + (M_1^2 - 1)^{1/2} + \frac{M_1}{M_2}(M_2^2 - 1)^{1/2}\left(\frac{X_2}{X_1}\right)^{(\gamma+1)/[2(\gamma-1)]}$$

## Appendix B

Snapshots of Excel and QBasic programs used to generate LA surface points. This program is based on Emanuel's formulation including equations 9 through 21.

| | A | B | C | D | E | F | G | H | I | J | K | L | M | N |
|---|---|---|---|---|---|---|---|---|---|---|---|---|---|---|
| 1 | $\alpha$ | $\gamma$ | M1 | M2 | $M_{A''}$ | M | X | X2 | X1 | $\gamma$ | P | S | K | $\Phi$ |
| 2 | -7.7301975 | -1.0000000 | 3 | 2 | 2.4551668365 | 3.0000000000 | 2.8 | 1.8 | 2.8 | 1.4 | 3 | 2.4 | 0.1667 | 0.204 |
| 3 | -7.6955219 | -0.9999833 | 3 | 2 | 2.4551668365 | 2.9972758342 | 2.7967 | 1.8 | 2.8 | 1.4 | 3 | 2.4 | 0.1667 | 0.204 |
| 4 | -7.6609850 | -0.9999332 | 3 | 2 | 2.4551668365 | 2.9945516684 | 2.7935 | 1.8 | 2.8 | 1.4 | 3 | 2.4 | 0.1667 | 0.204 |
| 5 | -7.6265863 | -0.9998501 | 3 | 2 | 2.4551668365 | 2.9918275025 | 2.7902 | 1.8 | 2.8 | 1.4 | 3 | 2.4 | 0.1667 | 0.204 |
| 6 | -7.5923255 | -0.9997341 | 3 | 2 | 2.4551668365 | 2.9891033367 | 2.7869 | 1.8 | 2.8 | 1.4 | 3 | 2.4 | 0.1667 | 0.204 |
| 7 | -7.5582021 | -0.9995856 | 3 | 2 | 2.4551668365 | 2.9863791709 | 2.7837 | 1.8 | 2.8 | 1.4 | 3 | 2.4 | 0.1667 | 0.204 |

| O | P | Q | R | S | T | U | V | W | X | Y |
|---|---|---|---|---|---|---|---|---|---|---|
| $\Theta_1$ | dM | $\beta$ | $\vartheta_M$ | $\vartheta_{A''}$ | $\vartheta_1$ | $\vartheta_2$ | $\beta_{A''}$ | $\beta_1$ | $\beta_2$ | Inc |
| 0 | 0.0027 | 2.828 | 0.86842952775 | 0.66442160491 | 0.86842952775 | 0.46041368208 | 2.242 | 2.828 | 1.732 | 200 |
| 9E-04 | 0.0027 | 2.826 | 0.86751176984 | 0.66442160491 | 0.86842952775 | 0.46041368208 | 2.242 | 2.828 | 1.732 | 200 |
| 0.002 | 0.0027 | 2.823 | 0.86659304414 | 0.66442160491 | 0.86842952775 | 0.46041368208 | 2.242 | 2.828 | 1.732 | 200 |
| 0.003 | 0.0027 | 2.82 | 0.86567334966 | 0.66442160491 | 0.86842952775 | 0.46041368208 | 2.242 | 2.828 | 1.732 | 200 |
| 0.004 | 0.0027 | 2.817 | 0.86475268542 | 0.66442160491 | 0.86842952775 | 0.46041368208 | 2.242 | 2.828 | 1.732 | 200 |
| 0.005 | 0.0027 | 2.814 | 0.86383105042 | 0.66442160491 | 0.86842952775 | 0.46041368208 | 2.242 | 2.828 | 1.732 | 200 |

```
'------------------------ useful constants  ----------------------------------
      g = 5 / 3: gm1 = g - 1: gp1 = g + 1: gm12 = gm1 / 2: fg = gm1 / gp1: fog = SQR(gp1 / gm1)
      pow = gp1 / 2 / gm1: gamma = g
      pi = 4 * ATN(1): raddeg = 180 / pi: degrad = 1 / raddeg

'---------------------------- left and right Mach numbers ------------------------
    M1 = 3: beta1 = SQR(M1 * M1 - 1): nu1 = fog * ATN(beta1 / fog) - ATN(beta1): bigx1 = 1 + gm12 * M1 * M1
    M2 = 2: beta2 = SQR(M2 * M2 - 1): nu2 = fog * ATN(beta2 / fog) - ATN(beta2): bigx2 = 1 + gm12 * M2 * M2
    deltaM = 0

    MAd = M1
    MBdd = M2
    fi = (nu1 - nu2) / 2: nuAdd = (nu1 + nu2) / 2
    Rstar = (M1 / fi) / (2 / gp1 * bigx1) ^ pow
    nuBd = fi + nu2

     '--------------coordinates of A and B ----------------------
     xA = (-1) / fi: yA = 0
     xB = (-1) * Rstar / M2 * (2 / gp1 * bigx2) ^ pow: yB = 0

     '--------------- coordinates of A' and A" from App A ------------
        xAd = xA - beta1: yAd = -1
    '       call xyplot xAd, yAd, 25
        muAdd = pi / 2 - 2 * ATN((TAN(nuAdd / 2)) ^ (1 / 3))
        MAdd = 1 / SIN(muAdd): bigxAdd = 1 + gm12 * MAdd * MAdd

        xAdd = (-1) * COS(fi) / fi * M1 / MAdd * (bigxAdd / bigx1) ^ pow: yAdd = xAdd * TAN(fi)


     '--------------- coordinates of B' ----------------------
        muBd = pi / 2 - 2 * ATN((TAN(nuBd / 2)) ^ (1 / 3))
        MBd = 1 / SIN(muBd): bigxBd = 1 + gm12 * MBd * MBd

        xBd = (-1) * COS(fi) / fi * M1 / MBd * (bigxBd / bigx1) ^ pow: yBd = xBd * TAN(fi)


    '----------------- coordinates of B" --------------------
        yBdd = (-1) * M1 / M2 * (bigx2 / bigx1) ^ pow
        xBdd = xB - yBdd * beta2

    '------------ intake length L -----------
    '     L = (-1) * (xAdd - xBdd)
```

## References


[1] Curran, E.T., Scramjet Engines: The first forty years. ISABE Paper 97-7005; XIII ISABE Conf. Sep 1997

[2] Molder, S., Curved Aerodynamic Shock Waves, A series of lectures presented at The Centre for Hypersonics, The University of Queensland, February 2012

[3] Van Wie, D. and Molder, S., Application of Busemann Inlet Designs for Flight at Hypersonic Speeds; 1992 Aerospace Design Conf.; AIAA 92-1210 (1992)

[4] George Emanuel, Lens Analogy, 2011, University of Oklahoma, Norman Oklahoma

[5] Busemann, A., Die achsensymmetrische kegelige Überschallströmung. Luftfahrtforschung 19, No. 4 137-144, 1944

[6] Courant, R. and Friedrichs, K.O., Supersonic Flow and Shock Waves, Interscience, 1948

[7] Molder, S. and Szpiro, E.J., Busemann Inlet for Hypersonic Speeds, Journal of Spacecraft and Rockets, Vol.3, No. 8 (1966)

[8] Molder, S., and Evgeny Timofeev, Hypersonic Air Intake Design for High Performance and Starting, Presented at the Von Karman Institute lecture series on: ENGINE INTAKE AEROTHERMAL DESIGN: SUBSONIC TO HIGH SPEED APPLICATIONS 14 to 17 Nov 2011

[9] Molder, S., A Benchmark for Internal Flow CFD Codes, 2011 (to be published)

[10] Anderson, John David., Hypersonic and high-temperature gas dynamics ISBN-13:978-1-56347-780-5


Note: Verbal communication have been obtained for unpublished reports by Molder, S.